Ten Years of TRMM/VIRS On-Orbit Calibrations and Multiyear Comparisons of VIRS and MODIS

CHENG-HSUAN LYU

Science Systems & Applications, Inc., Lanham, Maryland

WILLIAM L. BARNES

University of Maryland, Baltimore County, Baltimore, Maryland

(Manuscript received 8 January 2008, in final form 20 May 2008)

ABSTRACT

After 10 years of successful operation of the Tropical Rainfall Measuring Mission (TRMM)/Visible Infrared Scanner (VIRS), based on sensor performance, the authors have reexamined the calibration algorithms and identified several ways to improve the current VIRS level-1B radiometric calibration software. This study examines the trends in VIRS on-orbit calibration results by using lunar measurements to enable separation of the solar diffuser degradation from that of the VIRS Earth-viewing sensor and by comparing the radiometric data with two nearly identical Moderate Resolution Imaging Spectroradiometer (MODIS) instruments on board the NASA Earth Observing System (EOS) *Terra* and *Aqua* satellites. For the VIRS, with spectral bands quite similar to several of the MODIS bands, the integrated lunar reflectance data were measured, from January 1998 to March 2007, at phase angles ranging from 0.94° to 121.8°. The authors present trending of the lunar data over periods of 4 yr (*Aqua*/MODIS), 6 yr (*Terra*/MODIS), and 10 yr (TRMM/VIRS) and use these observations to examine instrument radiometric stability. The VIRS-measured lunar irradiances are compared with the MODIS-measured lunar irradiances at phase angles around 54°–56°. With the upcoming modified VIRS level-1B version 7 calibration algorithm, the VIRS, along with MODIS, should provide better references for intercalibrating multiple Earth-observing sensors.

1. Introduction

The Tropical Rainfall Measuring Mission (TRMM) spacecraft was launched in November 1997 for an originally designed 3-yr rainfall measuring mission (Simpson et al. 1996; Barnes et al. 1996). The currently operating Earth-viewing sensors aboard the TRMM are the Visible and Infrared Scanner (VIRS), the precipitation radar (PR), and the TRMM Microwave Imager (TMI). Using the PR and the TMI, TRMM provides a regular long-term set of precipitation measurements in the tropics and subtropics. VIRS was not designed to measure rainfall, but to provide cloud-top temperatures and structure that complement the measurements from the other sensors. This study will focus on the validation of the on-orbit calibration of VIRS over 10 yr using measurements from viewing the moon, the sun, and Earth. The VIRS instrument description and design, prelaunch and postlaunch calibration and characterization results, and a complete report of currently adopted radiometric calibration algorithms are described by Barnes et al. (1997), Kummerow et al. (1998), Barnes et al. (1998), Lyu et al. (2000), Lyu and Barnes (2003), and Barnes et al. (2000).

In this study, we use both *Terra*/Moderate Resolution Imaging Spectroradiometer (MODIS) and *Aqua*/MODIS as a semibenchmark for TRMM/VIRS based on the following four reasons: first, the designs for VIRS and MODIS are very similar, yet MODIS has significant improvements in sensor sensitivity, electronics, and calibration mechanisms. Second, nearly all of the MODIS solar and thermal bands have been performing well according to design specifications for 8.5 yr (*Terra*) and 6+ yr (*Aqua*). Third, intercomparisons show that *Aqua* and *Terra* MODIS differ in their respective bands, but these differences are mostly within their combined calibration uncertainties. Fourth, similar degradation trends have been observed (and prop-

Corresponding author address: Cheng-Hsuan Lyu, NASA Goddard Space Flight Center, Code 614.4, Greenbelt, MD 20771.
E-mail: lyu@neptune.gsfc.nasa.gov

DOI: 10.1175/2008JTECHA1110.1

© 2008 American Meteorological Society

erly corrected) for both VIRS and MODIS. For a detailed description of the MODIS calibration and its quality, see the MODIS Web site (http://www.mcst.ssai.biz/).

In our previous reports of VIRS calibration algorithms by Barnes et al. (2000), Lyu et al. (2000), and Lyu and Barnes (2003), the period (up to 4 yr) of the observed VIRS data was not sufficiently long and we were unable to perform a comprehensive validation of the VIRS algorithms. Specifically, when we compared calibrated VIRS radiances and reflectances with those from MODIS, the VIRS 1.61-μm band was about 10%–15% lower than the similar MODIS 1.64-μm band. This paper examines the performance of 10 yr of VIRS data in two steps. First, we perform checks of the currently adopted (VIRS version 6) radiometric calibration algorithms for both the reflected solar bands (0.62 and 1.61 μm) and the emitted thermal infrared bands (3.78, 10.83, and 12.03 μm). As mentioned by Lyu and Barnes (2003), any observed degradation might not be due to the sensor but to a change in the bidirectional reflectance distribution function (BRDF) of the solar diffuser. A way to determine the sensor degradation rate is to use the trending results of about 9 yr (111 months) of lunar measurements. We report the performance and propose updates of calibration algorithms for the VIRS solar and thermal bands in sections 2 and 3. Further, we present VIRS calibration uncertainties in section 4. Second, we compare calibrated VIRS reflectances and brightness temperatures with those of similar MODIS bands to determine differences in their coincident measurements. Both of these steps are important to the VIRS mission, since calibration is crucial in the use of VIRS radiances to obtain cloud and aerosol properties, which is how the VIRS radiances are used by the Clouds and the Earth's Radiant Energy System (CERES) team. In addition, an accurate calibration of the VIRS radiances is fundamental to their comparison with the radiances from past, current, and future Earth imagers. Also, the consistency in the sensor comparisons is fundamental to estimates of tropical precipitation both before and after the TRMM mission. We report these comparisons in section 5. The implications of the analyses and proposed updates are presented in concluding remarks in section 6.

2. Trends and algorithm updates for the VIRS solar bands

The reflected bands use a two-point linear calibration by periodically viewing the sun and space. These data determine the solar responsivities (gains) that, together with the sensor degradation rates (if applicable), are used to derive Earth-viewing radiances. Early studies using the coincident data measured in March 2001, performed by P. Minnis et al. (2002, personal communication) and Lyu and Barnes (2003), indicate that the radiances of the VIRS 0.62-μm band are comparable to those of the MODIS 0.65-μm band, but the radiances of the VIRS 1.61-μm band are about 15% smaller than those of the MODIS 1.64-μm band. Furthermore, the first 4 yr of on-orbit measured responsivities indicated an annual degradation rate for the 0.62-μm band of about 1.15% and no degradation for the 1.61-μm band. In most recent studies by Minnis et al. (2007), however, they conclude that the VIRS 0.62-μm band degrades at less than 0.1% yr^{-1}. After 10 yr of on-orbit TRMM/VIRS measurements, we now have sufficient data to revalidate the calibration algorithms as well as the sensor's performance.

a. Updated calibration algorithms for the solar bands

The spectral radiances for the two solar bands (i = 1, 2 = 0.62, 1.61 μm) from the Earth view (EV) are determined as follows:

$$L^i_{\mathrm{EV}} = \frac{\mathrm{DN}^i_{\mathrm{EV}} - \mathrm{DN}^i_{\mathrm{SV}}}{R_i\,\rho_i(\theta_{\mathrm{EV}})}, \tag{1}$$

$$R_i = \frac{[\mathrm{DN}^i_{\mathrm{SD}} - \mathrm{DN}^i_{\mathrm{SV}} - \Delta(\mathrm{DN}^i_{\mathrm{SD}} - \mathrm{DN}^i_{\mathrm{SV}})]\pi}{H^i_{\mathrm{sun}}(t)[0.1286 + 0.8\cos(\theta_{\mathrm{SD}})]\rho_i(\theta_{\mathrm{DV}})}, \tag{2}$$

where $\mathrm{DN}^i_{\mathrm{EV}}$, $\mathrm{DN}^i_{\mathrm{SV}}$, and $\mathrm{DN}^i_{\mathrm{SD}}$ are the digital counts (DN) from the EV, space view (SV), and solar diffuser (SD), which include corrections for variations in the scan mirror reflectance with angle of reflection and an electronics temperature correction. The $\rho_i(\theta_{\mathrm{EV}})$ is the reflectance of the scanning mirror, which is a function of the reflection angle, θ_{EV}, at which Earth is viewed; $\rho_i(\theta_{\mathrm{EV}})$ varies from 0.995 to 1.005 depending on the wavelength band and reflection angle (Barnes et al. 2000). Note in Eq. (1), the space view radiance is taken to be zero. Also, $\Delta(\mathrm{DN}^i_{\mathrm{SD}} - \mathrm{DN}^i_{\mathrm{SV}})$ is a correction term required because the baseline digital counts of SD (dark) and SV differ, and H^i_{sun} (t) is the spectral solar irradiance at the time of calibration [$H^1\mathrm{sun}(t_0) = 168.16$ and H^2_{sun} $(t_0) = 24.873$, mW cm^{-2} μm^{-1}, where t_0 is the time when the sun is at 1 A.U.]. To derive the above spectral solar irradiance, we adopted a model solar irradiance spectrum (Wehrli 1985) with a correction for the difference of the Earth–sun distance from 1 A.U. The θ_{SD} is the solar reflection angle of the diffuser (measured from diffuser normal); $0.1286 + 0.8[\cos(\theta_{\mathrm{SD}})]$, the empirically derived equation in the form of $a + \underline{b}$ $\cos(\theta_{\mathrm{SD}})$ from the measurements of BRDF of the dif-

fuser by Santa Barbara Remote Sensing (SBRS), represents the fraction of the reflected solar irradiance received by the detector for a given θ_{SD}. The $\rho_i(\theta_{DV})$ is the spectral reflectance of the scan mirror viewed from the diffuser at θ_{DV}, where $\rho_1(\theta_{DV}) = 0.8976$ and $\rho_2(\theta_{DV}) = 1.005$ (Barnes et al. 2000; Lyu and Barnes 2003). Note also that the original adopted $\rho_2(\theta_{DV})$, which was 0.9231 in the VIRS 1B01 version 6 (level 1B) algorithm, and was found to be in error. The original $\rho_1(\theta_{DV})$ is acceptable for the upcoming level-1B (version 7) algorithm. Using the above corrected $\rho_i(\theta_{DV})$ terms, we find that the initial (measured at launch) responsivities R_i should be 67.34 and 388.14 for the 0.62- and 1.61-μm bands, respectively. The original initial responsivities (Lyu and Barnes 2003) were 69.30 and 422.58. The adjustment of the responsivities, based on a degradation rate of 0.05% versus 1.15% yr^{-1} (see the following section), and the trending results for the 0.62-μm band minimize the radiance differences between MODIS and VIRS, especially for data after 2001.

Comparison of the reflectances from the VIRS 1.61-μm band and the MODIS 1.64-μm band indicate that the VIRS 1.61-μm band is lower by about 14% (see the following sections). We examined the calibration algorithm, but we did not find any clue to this problem until we reviewed the calibration documents and found that the BRDF of the SD and the reflectance of the scan mirror were not clearly defined. After determining the correct values of the scan mirror reflectance, we find that the reflectance measurements of the VIRS 1.61-μm band are comparable to those of the MODIS 1.64-μm band.

b. *Degradations using solar and/or lunar measurements*

Diffuser measurements occur about twice a month, and the exposure of the diffuser to the sun during each measurement lasts about 2 min. From these measurements, we calculate the responsivity R_i using the reflectance of the diffuser, the digital counts, and the irradiance from the sun [Eq. (2)]. The responsivities (or gains) of the VIRS 0.62- and 1.61-μm bands from 210 on-orbit solar calibrations are shown in Fig. 1. If there is no change in the diffuser reflectance on orbit, the changes in the diffuser-based measurements over time will track the changes in the sensor responsivity R_i. As shown in Fig. 1, only the 0.62-μm band exhibits a decrease in response over the VIRS mission. This is not surprising in that both optical components and diffuse surfaces have a tendency to degrade in the shorter wavelengths first. The 1.15% yr^{-1} loss in sensitivity (or responsivity) of the 0.62-μm band, measured while viewing the sun via the diffuser, cannot a priori be divided between the sensor and the diffuser. Since the EV data do not include the SD in the optical path, the question arises as to whether the decrease in responsivity is due to the sensor, to a change in the reflectance of the SD, or to both. Measurements of the moon, as with the EV measurements, do not include the SD in the optical path.

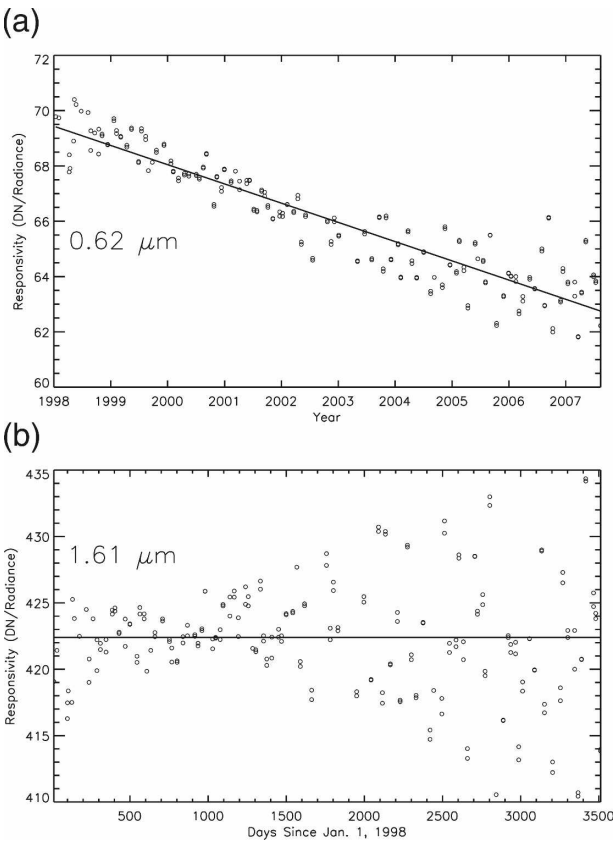

FIG. 1. Nine years of on-orbit responsivities for the VIRS (a) 0.62- and (b) 1.61-μm bands.

VIRS lunar measurements have been made near-monthly for over 9 yr. This 9-yr dataset, as mentioned previously, was collected to enable the separation of any solar diffuser degradation from that of the sensor. We have compiled 713 lunar measurements during 3400 observing days (Fig. 2). These data occur over a wide range of lunar phase angles, ranging from 0.94° to 121.8°. Besides the data presented in Fig. 2, we have removed about 300–500 partial lunar measurements. This is based on the fact that some of the lunar sequential measurements have significant drops (>10%) in the integrated spectral counts. This implies that the moon was not completely (only partially) detected. These partial data are found mostly at the beginning and end of the series of lunar scanning orbits and are probably due to obscuration by the edges of the SV port.

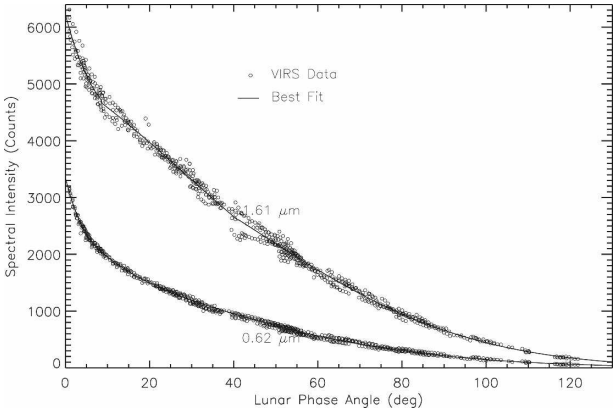

FIG. 2. Disk-integrated spectral intensity (counts) of the VIRS 0.62- and 1.61-μm data vs lunar phase angle.

Besides the partial lunar data at larger phase angles, one might worry that small phase angles could result in at least a partial lunar eclipse. This is because the moon and sun will be nearly in opposition as viewed from Earth, putting the moon partly in Earth's shadow. This would not be true for an observer at some distance from Earth, but TRMM is not at a high enough altitude to avoid the eclipse at small phase angles. However, even when the lunar phase was 0.94° on 26 May 2002, the moon had already moved outside the penumbra completely. Thus, the lunar data in this analysis represent completely scanned moons at the given phase angles. Note that the lunar data acquired after March 2007 are not usable, because there is an unexplained 10% drop in the integrated lunar counts for both the 0.62- and 1.61-μm bands. However, this decrease does not seem to affect the radiometric calibrations.

In Fig. 2, we have shown the best fit of the lunar spectral intensity versus phase for both the VIRS 0.62- and 1.61-μm bands. Because of lunar librations, the moon does not always show exactly the same face to Earth. There is more scatter in the VIRS 1.61-μm data than in the VIRS 0.62-μm data. Note that libration effects are changes in the lunar radiance as seen from the spacecraft due to variation in the side of the moon that faces Earth during the lunar observations. For the VIRS solar bands, libration effects are estimated to change the lunar brightness by as much as $\pm 5\%$ at 1.61 μm and by as much as $\pm 2\%$ at 0.62 μm. However, it is not certain that libration is the principal cause for this increased scatter.

After sorting out the time series of the VIRS lunar calibrations and normalizing the integrated values with the best-fit phase curve of Fig. 2, the quadratic best fit through the VIRS lunar spectral intensity data indicates that the VIRS sensor has been degrading approximately 0.05% yr^{-1} (see Fig. 3). Since the solar observations of the VIRS 0.62-μm band indicate a decrease in responsivity of 1.15% yr^{-1}, it follows that the SD reflectivity is decreasing approximately 1.1% yr^{-1}. Therefore, the next reprocessing of the VIRS data should include a time-dependent responsivity that decreases 0.05% yr^{-1}. The responsivity function for the VIRS 0.62-μm band due to the newly determined degradation rate should be 67.34–9.22466 $\times 10^{-5} \times$ (days since 1 January 1998).

To understand more about the performance of similar sensors, we compare the trending result using the lunar measurements of the *Terra*/MODIS and *Aqua*/MODIS 0.65-μm band with that of the VIRS 0.62-μm band in Fig. 3. We find that *Terra*/MODIS in its first five operational years degraded at a similar rate as VIRS. *Aqua*/MODIS, on the other hand, has a unique trending pattern. The *Aqua*/MODIS 0.65-μm band had an increase (as much as 3%) in its first 3 yr. However, in the recent 2 yr both *Terra*/MODIS and *Aqua*/MODIS seem to have similar degradation rates of 0.7% yr^{-1}. Because there are some bad detectors in the MODIS 1.64-μm band, together with significant (optical) signal leaks and cross-talk issues, we could not apply the lunar data for this band properly. The signal leaks and cross-talk problems have been minimized by adopting special data processing algorithms for the EV data, but not for the SV lunar data (because a sudden bright target appears in the SV for only a short time duration). Thus, we did not perform comparisons of sensor performance trending between the MODIS 1.64-μm band and the VIRS 1.61-μm band. Note the bad detectors found in both the *Terra*/MODIS and *Aqua*/MODIS 1.64-μm bands. The bad detectors in the *Terra*/MODIS were only observed in its early operational periods and were due to the use of specific configurations during on-orbit testing. These detectors return to normal after applying appropriate configurations. Please refer to Lyu et al. (2006) for a detailed description on how we adopt the scaling factors (m 0 and m 1 for MODIS scan mirror sides 0 and 1, respectively) to determine the MODIS sensor performance changes. Note also that for trending studies, both for the VIRS degradation data shown in Fig. 3 and the irradiance curves shown in Fig. 4, the VIRS data are derived by applying best fits to 9 yr of lunar measurements, whereas the MODIS results are based on individual lunar measurements.

In Fig. 4 we compare the MODIS lunar irradiance data at phase angles near 55° with VIRS lunar measurements at phase angles ranging from 0.94° to 121.8°. We normalized both datasets by dividing by the total integrated, band-averaged solar spectral irradiances. The normalized irradiance data from *Terra* are shown

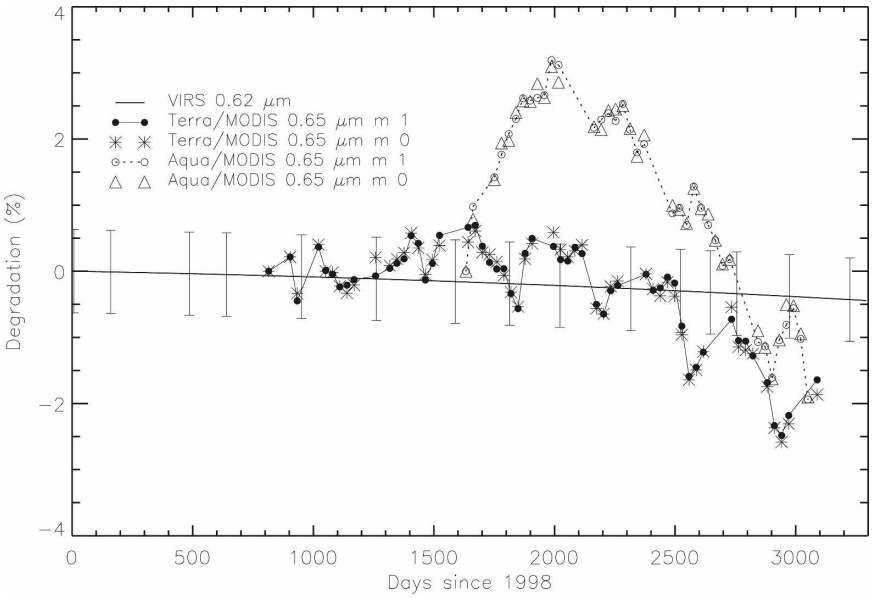

FIG. 3. Sensor performance trending of TRMM/VIRS, *Terra*/MODIS, and *Aqua*/MODIS vs days since 1998. The dates of the first lunar event for *Terra* and *Aqua* are 24 Mar 2000 and 20 Jun 2002, respectively. The 1σ error bar for VIRS is noted.

in Fig. 4a and those from *Aqua* in Fig. 4b. For comparison, the irradiance expected from an ideal Lambertian surface is also shown as a function of viewing angle. Also shown in the figure is the *Terra*/MODIS lunar irradiance at 22° phase angle, which was acquired during the second *Terra* deep space maneuver, implemented on 14 April 2003. We find that the derived lunar irradiances from both *Terra*/MODIS and *Aqua*/MODIS are comparable to, but slightly higher, than VIRS. Since different instruments view the moon at

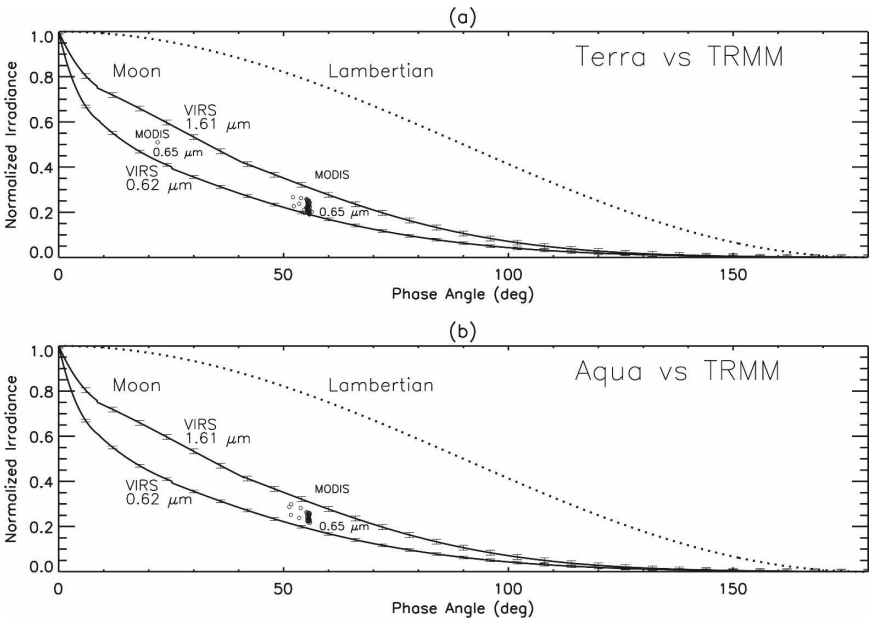

FIG. 4. Irradiance vs phase. The irradiance of the moon is represented by the best fits to the VIRS 0.62- and 1.61-μm data, normalized at 0° phase. The dotted line corresponds to the irradiance expected from a Lambertian surface. (a) *Terra* MODIS normalized irradiance vs VIRS; (b) *Aqua* MODIS normalized irradiance vs VIRS. The 1σ error bars for the VIRS 0.62- and 1.61-μm data are noted in (a) and (b).

somewhat different angles (e.g., the moon appears in waxing or waning phases), improved lunar models for TRMM/VIRS may have a significant impact on the derived irradiances.

3. Updates for VIRS thermal bands

During ground calibration, for the thermal bands, because of the nonlinear responses of the HgCdTe detectors, the digital counts from detector output were fit to a quadratic function of the measured radiance (Ld) as follows:

$$\mathrm{DN}_{Xc} = q_2 \times \mathrm{Ld}_X^2 + q_1 \times \mathrm{Ld}_X + \mathrm{DN}_0. \quad (3)$$

In Eq. (3), q_1, the dominant linear parameter, is different for each band and each scan line. It is determined on a scan-by-scan basis using the onboard blackbody. Here q_2 cannot be determined on orbit and is obtained from prelaunch measurements. Ld_X is the radiation incident on the detector, and X could be from the EV, the internal blackbody (BB), or the SV. Note that DN_{Xc} includes a correction (c) for drifts from the nominal electronics temperature T. When the input radiance is zero, the measured baseline count due to uncooled or imperfect devices (e.g., scan mirror, electronics, etc.) is DN_0. In this case, $\mathrm{DN}_0 = \mathrm{DN}_{\mathrm{SV}c}$.

For the VIRS thermal bands, the BB effective spectral radiance (L_{BBeff}) consists of three terms: 1) the radiance emitted from the BB itself; 2) radiance that is emitted from the cavity; and 3) radiance from the EV, but reflected by the BB. Moreover, our assumptions are that all sources can be described by a bandwidth averaged BB (using Planck's equation); the emissivity $\varepsilon_{\lambda\mathrm{BB}}$ is independent of wavelength across the bandwidth; and the "view" from the calibration BB consists of 95% cavity ($T_{\mathrm{cavity}} = T_{\mathrm{BB}} - 2$ K) and 5% Earth view ($T_{\mathrm{earth}} = 283$ K). Thus, the effective spectral radiance from the calibration BB can be described by the following equations:

$$\begin{aligned} L_{\mathrm{BBeff}} &= L_{\mathrm{BB}} + L_{\mathrm{BBcavity}} + L_{\mathrm{BBearth}} \\ &= \varepsilon_{\lambda\mathrm{BB}}\,\mathrm{BB}_n(T_{\mathrm{BB}}) + (1 - \varepsilon_{\lambda\mathrm{BB}})0.95\,\mathrm{BB}_n(T_{\mathrm{cavity}}) \\ &\quad + (1 - \varepsilon_{\lambda\mathrm{BB}})0.05\,\mathrm{BB}_n(T_{\mathrm{earth}}), \end{aligned} \quad (4)$$

where

$$\mathrm{BB}_n(T) = \frac{\sum_{\lambda\mathrm{lower}}^{\lambda\mathrm{upper}} \mathrm{BB}_\lambda(T)\Delta\lambda}{\sum_{\lambda\mathrm{lower}}^{\lambda\mathrm{upper}} \Delta\lambda}$$

and

$$\mathrm{BB}_\lambda(T) = \frac{2hc^2}{\lambda^5(e^{hc/\lambda KT} - 1)}. \quad (5)$$

Further, the incident radiation can be characterized by the reflectance of the mirror that directs the radiation from the source to the detector. That the mirror reflectance is not perfect implies that it is also a radiant source that must be taken into account when measuring the calibration BB, SV, and EV. We assume that L_{SV}, the space-view radiance, is zero. Also, the radiance from the uncooled optics is L_{BG}. Hence, we have

$$\begin{aligned} \mathrm{Ld}_{\mathrm{SV}} &= \varepsilon(\theta_{\mathrm{SV}})L_{\mathrm{mirror}} + L_{\mathrm{BG}} \\ &= [1 - \rho_n(\theta_{\mathrm{SV}})]\mathrm{BB}_n(T_{\mathrm{mirror}}) + L_{\mathrm{BG}}, \end{aligned} \quad (6)$$

$$\begin{aligned} \mathrm{Ld}_{\mathrm{BB}} &= \rho_n(\theta_{\mathrm{BB}}) \times L_{\mathrm{BBeff}} + [1 - \rho_n(\theta_{\mathrm{BB}})]\mathrm{BB}_n(T_{\mathrm{mirror}}) \\ &\quad + L_{\mathrm{BG}}, \end{aligned} \quad (7)$$

$$\begin{aligned} \mathrm{Ld}_{\mathrm{EV}} &= \rho_n(\theta_{\mathrm{EV}}) \times L_{\mathrm{EV}} + [1 - \rho_n(\theta_{\mathrm{EV}})]\mathrm{BB}_n(T_{\mathrm{mirror}}) \\ &\quad + L_{\mathrm{BG}}, \end{aligned} \quad (8)$$

where $\rho_n(\theta_{\mathrm{BB}})$, $\rho_n(\theta_{\mathrm{SV}})$, and $\rho_n(\theta_{\mathrm{EV}})$ correspond to the reflectances for measurement at θ_{BB}, θ_{SV}, and θ_{EV}, respectively. All quantities on the rhs of Eqs. (6) and (7) can be determined from flight measurements or stored in ground (laboratory)-based lookup tables, except that L_{BG} is unknown. Fortunately, $\mathrm{Ld}_{\mathrm{BB}} - \mathrm{Ld}_{\mathrm{SV}}$ is independent of L_{BG}.

To determine the calibration coefficients, q_1, we can calculate the radiance from the BB ($L_{\mathrm{BB}} = \mathrm{Ld}_{\mathrm{BB}} - \mathrm{Ld}_{\mathrm{SV}}$). Using $\mathrm{Ld}_{\mathrm{BB}} - \mathrm{Ld}_{\mathrm{SV}} = \rho_n(\theta_{\mathrm{BB}})\,L_{\mathrm{BBeff}} + [\rho_n(\theta_{\mathrm{SV}}) - \rho_n(\theta_{\mathrm{BB}})]\,\mathrm{BB}_n(T_{\mathrm{mirror}})$, we have

$$\begin{aligned} \mathrm{DN}_{\mathrm{EV}c} &= q_2(\mathrm{Ld}_{\mathrm{EV}} - \mathrm{Ld}_{\mathrm{SV}})^2 + q_1(\mathrm{Ld}_{\mathrm{EV}} - \mathrm{Ld}_{\mathrm{SV}}) \\ &\quad + \mathrm{DN}_0. \end{aligned} \quad (9)$$

Solving for q_1 we have

$$q_1 = \frac{\mathrm{DN}_{\mathrm{BB}c} - \mathrm{DN}_{\mathrm{SV}c}}{\mathrm{Ld}_{\mathrm{BB}} - \mathrm{Ld}_{\mathrm{SV}}} - q_2(\mathrm{Ld}_{\mathrm{BB}} - \mathrm{Ld}_{\mathrm{SV}}). \quad (10)$$

Hence, once L_{BBeff} and other terms have been determined and the $\mathrm{DN}_{\mathrm{BB}c}$, $\mathrm{DN}_{\mathrm{SV}c}$ acquired, Eq. (10) can be used to determine q_1 for each channel.

When measuring the scene radiance (i.e., the DN) from Earth view, we have

$$\begin{aligned} \mathrm{DN}_{\mathrm{EV}c} &= q_2(\mathrm{Ld}_{\mathrm{EV}} - \mathrm{Ld}_{\mathrm{SV}})^2 + q_1(\mathrm{Ld}_{\mathrm{EV}} - \mathrm{Ld}_{\mathrm{SV}}) \\ &\quad + \mathrm{DN}_0. \end{aligned} \quad (11)$$

Note that if $\mathrm{Ld}_{\mathrm{EV}}$ is the same as $\mathrm{Ld}_{\mathrm{SV}}$, then $\mathrm{DN}_{\mathrm{EV}c} = \mathrm{DN}_{\mathrm{SV}c} = \mathrm{DN}_0$. Solving for $\mathrm{Ld}_{\mathrm{EV}}$ we get

$$\begin{aligned} \mathrm{Ld}'_{\mathrm{EV}} &= \mathrm{Ld}_{\mathrm{EV}} - \mathrm{Ld}_{\mathrm{SV}} \\ &= \frac{-q_1 + \sqrt{q_1^2 - 4q_2(\mathrm{DN}_0 - \mathrm{DN}_{\mathrm{EV}c})}}{2q_2}. \end{aligned} \quad (12)$$

Therefore, adopting Eqs. (6) and (8), the EV scene radiance is found to be

$$\mathrm{Ld}_{\mathrm{EV}} = \{\mathrm{Ld}'_{\mathrm{EV}} + [\rho_n(\theta_{\mathrm{EV}}) - \rho_n(\theta_{\mathrm{SV}})]\mathrm{BB}_n(T_{\mathrm{mirror}})\}/\rho_n(\theta_{\mathrm{EV}}). \quad (13)$$

This is a description of the current (version 6) VIRS level-1B algorithm (see also Barnes et al. 2000) for the VIRS thermal bands.

4. VIRS calibration uncertainties

The radiometric accuracies calculated prelaunch for the in-flight calibration of the VIRS solar bands (0.62 and 1.61 μm) are about 5.6% (TRMM/VIRS 1996). The important uncertainty contributors include calibration sources (either from the solar diffuser or the lunar measurements), scan mirror reflection angle, stray light, out-of-band spectral effects (imperfect spectral filters), and out-of-field (near field) response. The most significant error source comes from the calibration source (4.0%). The next one is from out-of-field effects (3.0%), and then the out-of-band spectral effects (2.0%). Note that the out-of-field error is due to the detection of radiance outside the field of view of the VIRS 6-mrad pixel and is most likely due to light scattered off the primary mirror. The uncertainty contribution from the mirror reflectance is small (less than 1%). Other instrumental uncertainties are also small. Note also that the uncertainty contributors are assumed independent of each other. The root sum square (RSS) of the individual uncertainty contributions results in the total radiometric uncertainty (e.g., 5.6% for the VIRS solar bands). The individual errors are a combination of measurements (i.e., standard lamp orientation, diffuser-to-lamp distance, etc.) and modeled results (i.e., scattered light, wavelength calibration, etc.). The various elements can be found in appendix A of TRMM/VIRS (1996).

The radiometric accuracies calculated prelaunch for the in-flight calibration of the thermal bands (3.78, 10.83, and 12.03 μm) are about 2.7% (TRMM/VIRS 1996). The primary uncertainty contributors include scan mirror reflection angle and in-band and out-of-band spectral effects. The uncertainty in the radiance from the calibration source is less than 0.9% for the 3.78-μm band and is less than 0.5% for both the 10.83- and 12.03-μm bands. In terms of temperature for an Earth scene at 300 K, the uncertainties are about 2 K. From measurements on orbit by Lyu et al. (2000), the reflectances for the 10.83- and 12.03-μm bands differ by up to 2%, but the prelaunch reflectances adopted from MODIS measurements for these bands are the same (Barnes et al. 2000). The uncertainty of the on-orbit reflectances would be additional to the primary sources of uncertainty for the VIRS thermal radiances.

5. Comparisons of VIRS and MODIS

Radiometric comparisons of the five spectral bands of TRMM/VIRS (level-1B version 6) have been made with similar bands from the *Terra*/MODIS (level-1B version 5) by using coincident datasets measured in March 2001, June 2002, September 2003, December 2004, and April 2007 (see Figs. 5–7). The Satellite Tool Kit (STK) from Analytic Graphics Inc. (www.agi.com) was used to find coincident times and nadir geolocations for VIRS and MODIS. A similar approach on how to determine the exact crossover of two spacecrafts/sensors has been presented by Lyu and Barnes (2003).

For low-flying satellites such as TRMM, solar drag is always an issue. Thus, for the STK satellite propagation analyses new ephemeris data must be carefully selected and adopted for both the TRMM and *Terra* spacecraft almost every day. After locating 20–40 crossovers of VIRS and MODIS in a month, the data around these nadir crossovers (within a 1.0° × 1.2° region) were gridded into 0.2° latitude × 0.4° longitude regions. This results in 300–600 near-nadir regions, which were observed in both day and night. The pixel size of VIRS is 6 mrad [i.e., 2.1 km (TRMM at 350 km) or 2.41 km (TRMM at 402 km after 24 August 2001)]. For MODIS, whose pixel size is 0.35 mrad (0.25 km) for the 0.65-μm band, we choose the data product with an aggregated pixel size of 1 km. Hence, in the 0.2° × 0.4° region there are 137–270 data points from VIRS and 770–970 data points from MODIS. The time differences of the crossovers between VIRS and MODIS are all within 2 min and a few seconds. This ensures that there are no extra uncertainties resulting from scene changes (cloud motion). Note that both the *Terra* and *Aqua* are polar-orbiting satellites in sun-synchronous orbits at a nominal altitude of 705 km, inclined at about 98.2°. The TRMM is in a non-sun-synchronous orbit, at 35° inclination. Also, the geolocation (latitude, longitude) is designated by the center of each pixel (or aggregated MODIS pixel). The actual projected map of two different sensors may display some offsets in (latitude, longitude) location. In these comparisons, we assume that the effects resulting from the geolocation mapping offsets are negligible.

In Fig. 5, we present comparisons of the reflectance data of similar solar bands obtained from VIRS version 6 and MODIS version 5 in the years between 2001 and 2006. For the VIRS 0.62-μm band, we adopted a radi-

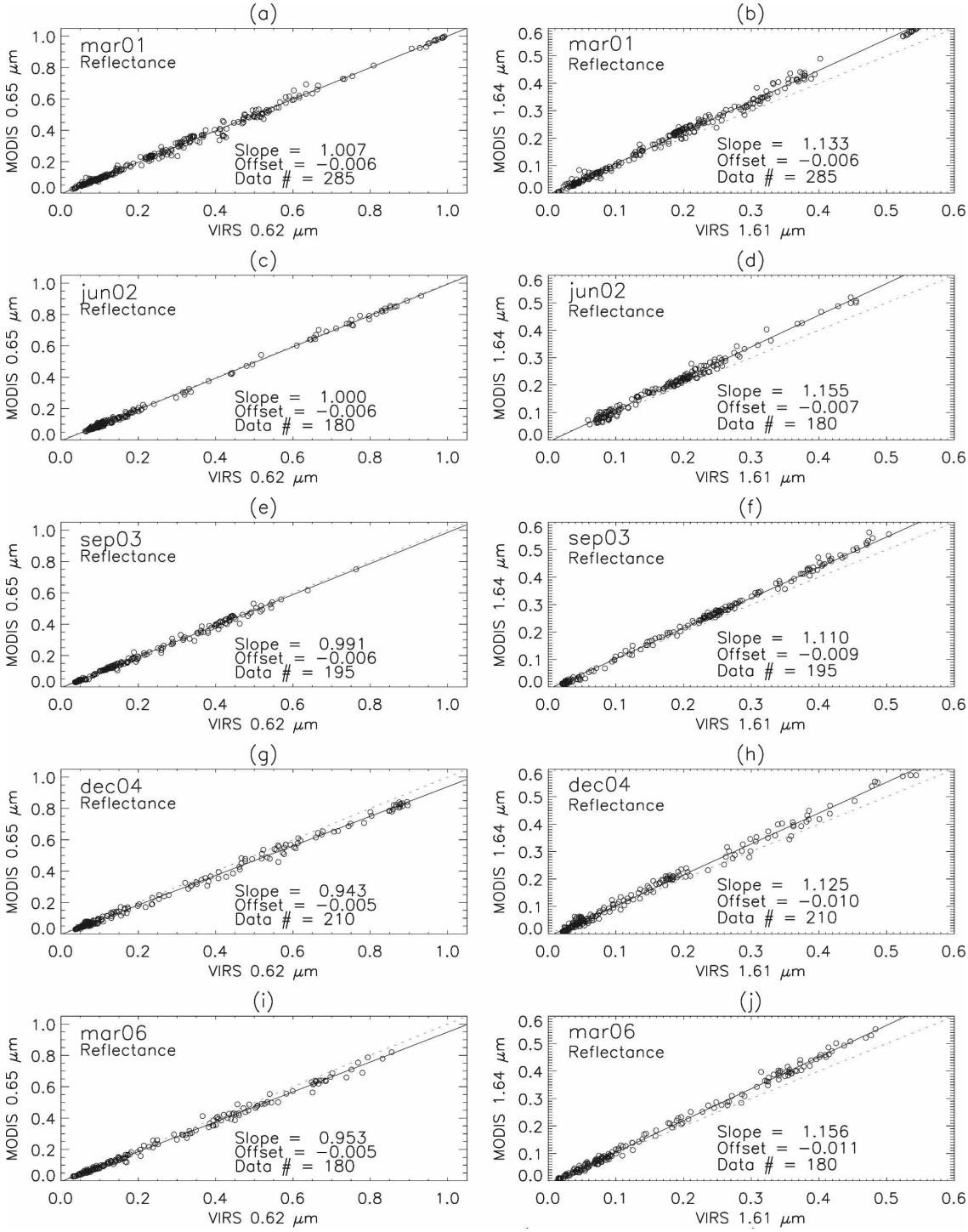

FIG. 5. Radiometric comparisons of TRMM/VIRS version 6, *Terra*/MODIS version 5 data observed in March 2001, June 2002, September 2003, December 2004, and March 2006.

ance degradation rate of 1.15% yr^{-1} in the version 6 data products. Lyu and Barnes (2003) derived this degradation rate from the first 4 yr of solar diffuser measurements but found that the lunar calibration data were not adequate to establish the degradation of the sensor. If MODIS is assumed to have maintained its original sensor performance, then the use of an inappropriate sensor degradation rate may be the reason

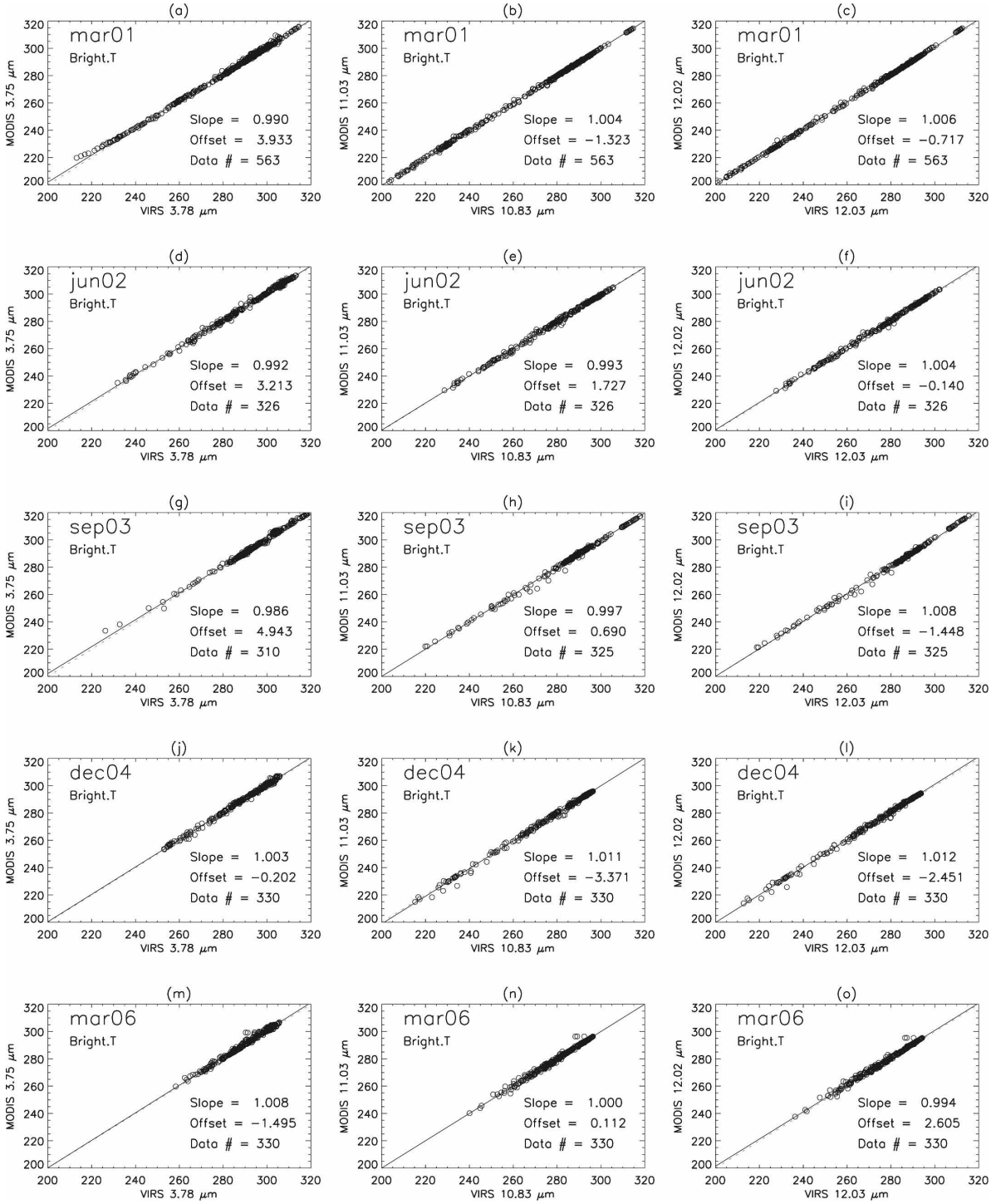

FIG. 6. Brightness temperature comparisons of TRMM/VIRS version 6, *Terra*/MODIS version 5 data observed in March 2001, June 2002, September 2003, December 2004, and March 2006.

why the VIRS 0.62-μm band calibration results start to deviate from the MODIS 0.65-μm band in the year 2003. For the VIRS 1.61-μm band, as indicated in earlier studies, the derived reflectance is consistently lower than the MODIS 1.64-μm band by about 14%. Note that the solid line is the best fit to the data and the dotted line represents a slope of 1 with zero offset.

In Fig. 6, we present comparisons of the brightness

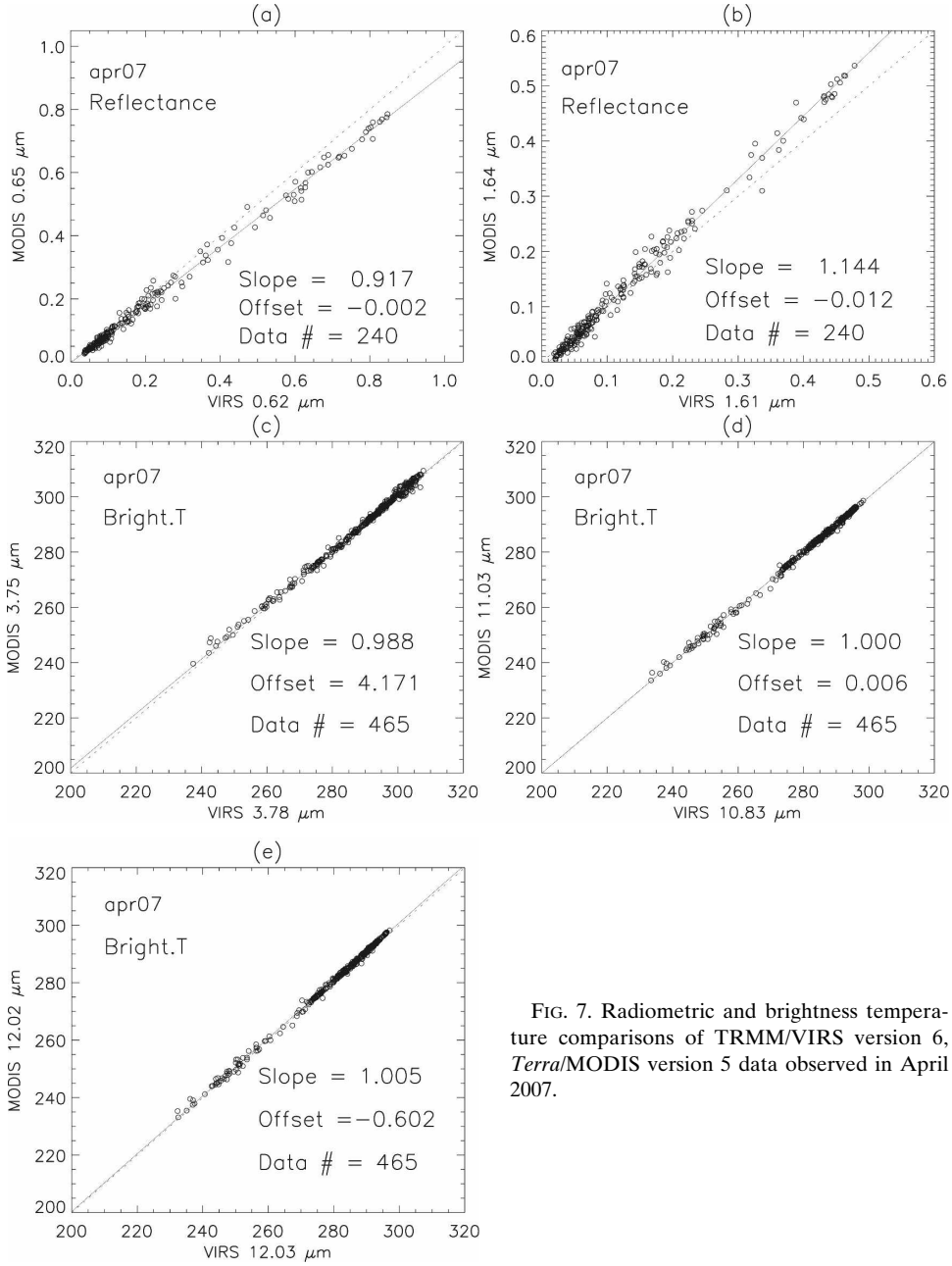

FIG. 7. Radiometric and brightness temperature comparisons of TRMM/VIRS version 6, *Terra*/MODIS version 5 data observed in April 2007.

temperatures of similar thermal bands obtained from VIRS version 6 and MODIS version 5 in the years between 2001 and 2006. We find that all three VIRS thermal bands (3.78, 10.83, and 12.03 μm) are comparable to the MODIS thermal bands at 3.75, 11.03, and 12.02 μm, respectively. Note that MODIS has a larger calibration range, namely, the derived brightness temperatures of the EV scenes are between 168.9 and 337.7 K (*Aqua*) and between 168.9 and 336.4 K (*Terra*) for the 3.75-μm band, between 92.7 and 339.5 K (*Aqua*) and 92.6 and 398.9 K (*Terra*) for the 11.03-μm band, and between 87.7 and 341.3 K (*Aqua*) and 87.7 and 396.5 K (*Terra*) for the 12.02-μm band (MODIS Characterization Support Team 2007, personal communication). For the VIRS thermal bands, we can only measure scene brightness temperatures between 180 and 330 K. Moreover, MODIS has 12 bits of digitization versus 10–11 bits for VIRS. Consequently, MODIS has better precision in measuring reflectances and brightness temperatures.

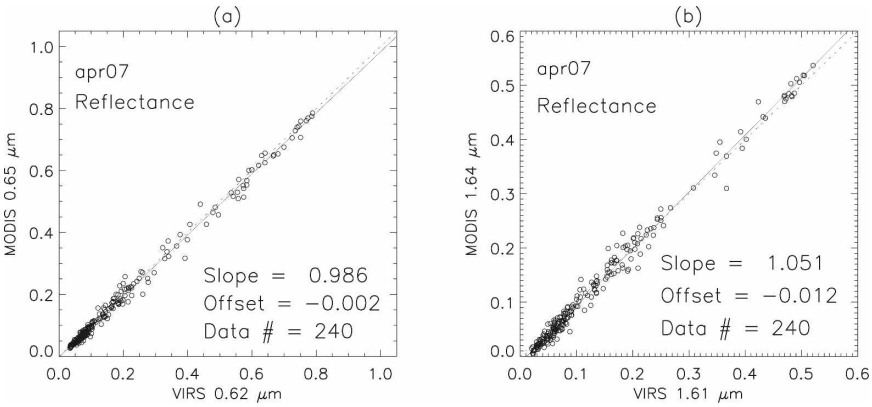

FIG. 8. Radiometric comparisons of TRMM/VIRS version 7 and *Terra*/MODIS version 5 data observed in April 2007.

In Fig. 7, we present comparisons of the reflectance as well as brightness temperatures of similar bands obtained from VIRS version 6 and MODIS version 5 in April 2007. The results are comparable to those presented in Figs. 5 and 6. As explained in sections 3 and 4, we have found several possible improvements for the VIRS radiometric calibrations. First, the lunar measurements imply that the degradation rate for the VIRS 0.62-μm band should be 0.05% yr^{-1}. Second, the responsivity for the VIRS 1.61-μm band should be 388.14. These changes will be incorporated in the upcoming VIRS level-1B (version 7) calibration algorithms.

In Fig. 8, we present comparisons of the reflectances of similar bands obtained using the proposed VIRS version 7 and MODIS version 5 for April 2007. After adopting the VIRS version 7 algorithm, to be implemented operationally around 2008–09, we find that the VIRS solar bands should agree with similar MODIS bands, within their uncertainties. The VIRS thermal bands are not shown, since their calibration algorithm is the same as for version 6.

6. Concluding remarks

In comparing VIRS level-1B version 6 data with MODIS version 5 data the VIRS 0.62- and MODIS 0.65-μm band comparison is reasonable and the trend of the difference is consistent with the responsivity correction equation. The measured reflectances of the VIRS 0.62-μm band deviate from those of the MODIS 0.65-μm band and increase with time after the launch of TRMM/VIRS. This is due to the use of the degradation rate of 1.15% yr^{-1} resulting from the SD on-orbit measurements. The lunar data should enable separation of any solar diffuser degradation from that of the VIRS sensor. However, in our last report (Lyu and Barnes 2003), we did not have sufficient lunar measurements to determine precise degradation rates. We assumed that the degradation in the response of the 0.62-μm band was due solely to the sensor.

A study of the trend in lunar reflectance measurements over 9 yr indicates that the VIRS sensor is degrading about 0.05% yr^{-1} for the 0.62-μm band. Moreover, with this revised degradation rate (in the upcoming level-1B version 7 algorithm), the radiometric measurements of both the VIRS 0.62- and the MODIS 0.65-μm band are comparable.

After adopting corrected scan mirror reflectance values in the level-1B version 7 algorithm, the reflectance measurements of the VIRS 1.61-μm band are comparable to those of the MODIS 1.64-μm band. The remaining 5% difference is mostly due to differences in the sensors in terms of bandwidths, wavelength centers, detection or saturation limits, and the intrinsic uncertainty in the measurements.

The Robotic Lunar Observatory (ROLO) model is being developed (T. Stone 2007, personal communication) to establish a spectral irradiance model of the moon to account for variations with lunar phase, lunar librations, and the location of Earth-orbiting spacecraft. This program is capable of characterizing the brightness of the moon for the on-orbit calibration of Earth-sensing imaging radiometers. As an alternative to the approach presented here, the ROLO model should be able to determine integrated lunar irradiances for each of the VIRS lunar measurements. This will enable us to improve our on-orbit radiometric calibrations and to more directly track changes in sensor response.

The TRMM/VIRS thermal bands are comparable to similar MODIS bands. The current VIRS version 6 thermal band calibration algorithm will be retained for the upcoming version 7 data products. We expect, with

the version 7 algorithms, that VIRS should provide significant improvements for intercalibrating multiple Earth-observing sensors.

Acknowledgments. We would like to express our thanks for technical support from the TRMM Science Data and Information System (TSDIS), especially, Yong Zhang, who provided VIRS level-1B operational codes and SYBASE database tool kits, which helped us greatly in checking modified level-1B data products. The authors thank R. Barnes for many useful discussions regarding the current calibration algorithm, and also wish to thank Jack Xiong and J. Sun for technical support from the MODIS Characterization Support Team (MCST). We appreciated reviewers' comments, which helped us greatly in improving the manuscript.

REFERENCES

Barnes, R., W. Barnes, C.-H. Lyu, and J. Gales, 2000: An overview of the VIRS radiometric calibration algorithm. *J. Atmos. Oceanic Technol.,* **17,** 395–405.

Barnes, W. L., R. A. Barnes, and A. W. Holmes, 1996: Characterization and calibration results from the Visible and Infrared Scanner (VIRS) for the Tropical Rainfall Measuring Mission (TRMM). *Advanced and Next-Generation Satellites II,* H. Fujisada, G. Calamai, and M. N. Sweeting, Eds., International Society for Optical Engineering (SPIE Proceedings, Vol. 2957), 266–276.

——, R. Barnes, and A. Holmes, 1997: Characterization and calibration results from the Visible and Infrared Scanner (VIRS) for the Tropical Rainfall Measuring Mission (TRMM). *Advanced and Next Generation Satellites,* H. Fujisada et al., Eds., International Society for Optical Engineering (SPIE Proceedings, Vol. 2957), 266–276.

——, T. Pagano, and V. Salomonson, 1998: Prelaunch characteristics of the Moderate Resolution Imaging Spectroradiometer (MODIS) on EOS-AM1. *IEEE Trans. Geosci. Remote Sens.,* **36,** 1088–1100.

Kummerow, C., W. Barnes, T. Kozu, J. Shiue, and J. Simpson, 1998: The Tropical Rainfall Measuring Mission (TRMM) sensor package. *J. Atmos. Oceanic Technol.,* **15,** 809–817.

Lyu, C.-H., and W. Barnes, 2003: Four years of TRMM/VIRS on-orbit calibrations and characterization using lunar models and data from *Terra*/MODIS. *J. Atmos. Oceanic Technol.,* **20,** 333–347.

——, ——, and R. Barnes, 2000: First results from the on-orbit calibrations of the VIRS for the TRMM. *J. Atmos. Oceanic Technol.,* **17,** 385–394.

——, J. Sun, X. Xiong, and W. Barnes, 2006: Multiyear lunar observations from TRMM/VIRS, *Terra*/MODIS and *Aqua*/MODIS. *Remote Sensing and Modeling of Ecosystems for Sustainability III,* W. Gao and S. L. Ustin, Eds., International Society for Optical Engineering (SPIE Proceedings, Vol. 6298), 629 811–629 819.

Minnis, P., D. R. Doelling, L. Nguyen, W. F. Miller, and V. Chakrapari, 2007: Assessment of the visible channel calibrations of the VIRS on TRMM and MODIS on *Aqua* and *Terra*. *J. Atmos Oceanic Technol.,* **25,** 385–400.

Simpson, J., C. Kummerow, W.-K. Tao, and R. Adler, 1996: On the Tropical Rainfall Measuring Mission (TRMM). *Meteor. Atmos. Phys.,* **60,** 19–36.

TRMM/VIRS, 1996: CDRL 507, final technical description document. Contract NAS5-32044, 20 pp.

Wehrli, C., 1985: Extraterrestrial solar spectrum. PMOD/WRC Publication 615, 26 pp.